Plate-like precipitate effects on plasticity of Al-Cu alloys at micrometer to sub-micrometer scales

Peng Zhang, Jian-Jun Bian, Jin-Yu Zhang, Gang Liu, Jérôme Weiss, Jun Sun

Materials and Design 188 (2020) 108444

Contents lists available at ScienceDirect

Materials and Design

journal homepage: www.elsevier.com/locate/matdes

Plate-like precipitate effects on plasticity of Al-Cu alloys at micrometer to sub-micrometer scales

Peng Zhang [a], Jian-Jun Bian [a], Jin-Yu Zhang [a], Gang Liu [a,*], Jérôme Weiss [b,*], Jun Sun [a,*]

[a] State Key Laboratory for Mechanical Behavior of Materials, Xi'an Jiaotong University, Xi'an 710049, China
[b] IsTerre, CNRS/Université Grenoble Alpes, 38401 Grenoble, France

HIGHLIGHTS

- Different structures are constructed in Al-Cu pillars by adjusting the ratio of sample and plate-like precipitate diameters.
- A complex sample size dependent plasticity is observed, showing three distinct regimes.
- The intermittent plasticity can be effectively inhibited when the plate-shaped precipitates penetrate the entire sample.
- The relation between power-law exponent of strain burst distribution and wildness is universal.

GRAPHICAL ABSTRACT

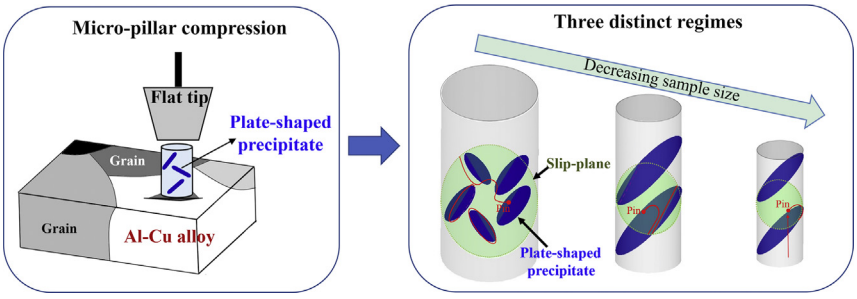

ARTICLE INFO

Article history:
Received 27 August 2019
Received in revised form 17 December 2019
Accepted 18 December 2019
Available online 03 January 2020

Keywords:
Dislocation dynamics
Size effects
Plastic fluctuations

ABSTRACT

The continuous miniaturization of modern electromechanical systems calls for a comprehensive understanding of the mechanical properties of metallic materials specific to micrometer and sub-micrometer scales. At these scales, the nature of dislocation-mediated plasticity changes radically: sub-micrometer metallic samples exhibit high yield strengths, however accompanied by detrimental intermittent strain fluctuations endangering structural stability. In this paper, we studied the effects of plate-like θ'-Al_2Cu precipitates on the strength and plastic fluctuations of Al-Cu alloys from micro-pillar compression testing. The particularity of our samples is that the plate-like precipitates have diameters commensurate with the external size of the Al-Cu micro-pillars. Our results show that these plate-like precipitates can strengthen the materials through the Orowan mechanism at large sample size. However, the breakdown of the mean-field pinning landscape weakens its suppression effect on plastic intermittency. On the other hand, the plastic intermittency can be inhibited efficiently at small sample size by using the plate-like θ'-Al_2Cu precipitates penetrating the entire micro-pillar, in association with the presence of {100}-slip traces along the coherent precipitate/Al matrix interface and enhanced strain isotropy. Besides these experimental observations, we also aim to extract the laws common in different Al alloys, and address the specific plastic mechanisms for Al-Cu micro-crystals.

Data availabilityThe data used to support the findings of this study are available from the corresponding author upon request.

1. Introduction

Over recent years, the structural analysis and design of metallic structures in the field of micro- and nano-electromechanical systems (MEMS and NEMS) highlighted the need to investigate the specificity

* Corresponding authors.
E-mail addresses: lgsammer@xjtu.edu.cn (G. Liu), jerome.weiss@univ-grenoble-alpes.fr (J. Weiss), junsun@xjtu.edu.cn (J. Sun).

https://doi.org/10.1016/j.matdes.2019.108444

of the mechanical properties of metallic materials at those scales [1,2]. The vast amount of work on single crystals published during the last decade [3–8] revealed several size effects characterizing micro-plasticity: (i) a "smaller is stronger" effect, caused by novel plastic mechanisms commonly referred to "source truncation" [9–12] and "dislocation starvation" [13,14]; (ii) a modification of hardening mechanisms, from classical forest-hardening at large length scales to exhaustion hardening [9,15,16]: to sustain the flow in the case where weak dislocation sources are exhausted, much higher stress is required for the activation of the stronger, truncated ones. These studies depicted a different landscape, away from conventional engineering, and paved the way towards size-dependent design [1].

Besides an enhanced plastic yield stress, another specific feature of sub-μm plasticity is the intermittent character of plastic flow, which manifests itself directly on the stress-strain curves through discrete strain bursts with a broad range of sizes following power-law tailed distributions [17–25]. These collective effects and dislocation avalanches are rooted in the long ranged elastic interactions between dislocations, hence challenging some fundamental aspects of classical plasticity theory based on the behavior of individual dislocations, or which is assuming an average response of dislocation ensembles [5,26–28]. They have been regarded as a common feature of small sized single crystals, prevailing not only in face-centered cubic (FCC), but also in body-centered cubic (BCC) and hexagonal closed-packed (HCP) structures [8,29–32]. From the engineering viewpoint, the plastic fluctuations are unwelcome due to their unpredictable nature and the possibility for large avalanches to span the whole system size [19]. Giving a practical example, the mass production of metallic patterns with high resolution and quality (e.g., ultra-smooth surfaces) represents a substantial challenge, partly limited by undesired morphological fluctuations resulting from stochastic dislocation avalanches [33]. Thus, developing methodologies to tame the detrimental effects of plastic fluctuations in a predictable and quantitative manner is of critical importance for the structural analysis and design of metallic structures at small scales [19].

Some previous investigations [34–36] suggested that smooth plastic flow can be achieved via the introduction of quenched disorder, which occurs through a thwarting of the long-range interactions between dislocations [17], thereby providing the potential for inhibiting intermittency. The advantages of using precipitates to inhibit plastic intermittency, compared with other effective methodologies such as grain boundary engineering and coating for small samples [37–39], not only come from the fact that precipitation processes (aging treatment) are well controlled [40], but also from the variety of precipitates that can be utilized. However, these previous studies [17,34–36] on inhibiting plastic fluctuations mainly focus on the effects of obstacles or precipitates with internal length scales (individual disorder size and disorder spacing) much smaller than the dimension of material. On the other hand, the possibility to utilize precipitates with internal length scales comparable to, or even larger than, the external size of small technological devices has not been addressed. In this study, we systematically explore strength and plastic fluctuations in small-sized Al-Cu single crystals containing plate-like θ'-Al_2Cu precipitates. The average precipitate diameter is about 1 μm, comparable with the inter-particle spacing and the diameter of our micro-pillars (300 nm ≤ L ≤ 4000 nm). We perform the micro-pillar compression tests, examine to what extent the interactions between internal and external length scales fit the previously proposed theoretical framework [17,41], and show how to take advantage of such type of disorder. The laws common in different Al alloys and the specific plastic mechanisms for Al-Cu micro-crystals are summarized.

2. Experimental procedures

Two kinds of casting Al-Cu alloys, one with a composition of Al-2.5 wt% Cu (abbreviated Al-2.5Cu) and the other with Al-4.0 wt% Cu (Al-4.0Cu), were studied. The two alloys were solutionized at 793 K for 4 h, followed by a cold-water quench and immediately aged at 523 K for 8 h. Precipitates in the aged alloys were quantitatively characterized by standard transmission electron microscopy (TEM) (Fig. 1a and b) and high-resolution transmission electron microscopy (HRTEM). An electron backscatter diffraction (EBSD) detector (Oxford, HKLNordlys) integrated with the focus ion beam (FIB) system was used to probe the crystal orientation on the electro-polished surfaces of the aged samples (Fig. 1d). The electron beam with 25 kV and 2.1 nA were used, and the step size was set as 2 μm, in consideration of the mm-sized grain in our casting alloys. A grain with its normal along the [110]-direction, an orientation identical to the Al-alloys micro-pillars we studied before [17], was selected to fabricate micro-pillars by FIB micro-machining. Micro-pillars were prepared with a diameter ranging from 300 to 4000 nm at mid sample height, with an aspect ratio of ~ 3:1 (see Fig. 1e and f).

The ex-situ micro-compression tests were performed on a nano-indentation system (Hysitron Ti 950) with a 10 μm flat diamond tip. Following our previous test conditions [17], the micro-pillars were compressed at room temperature under a displacement-controlled mode, with a strain rate of ~2×10^{-4} s^{-1} up to 18% engineering strain. In-situ TEM compression testing was also performed on [110]-oriented Al-2.5Cu alloy micro-pillars, by using a nano-indentation system (Hysitron Pi 95) inside the TEM chamber. Further details on micro-pillar fabrication and the mechanical testing methodology can be referred to the Refs. [42–45]. To evaluate the total strengthening contribution from obstacles, tensile tests were performed on bulk polycrystalline Al-Cu by using a servohydraulic Instron-1195 testing machine, with a same strain rate as in micro-compression tests. The tensile specimens were dog-bone shaped, with a gauge size of 15 mm in diameter and a length of 75 mm.

3. Characterization of tested materials

In this section, we characterize the tested materials in terms of characteristic length scales and pinning strength of precipitate arrays, which are crucial to understand the experimental results.

3.1. Characteristic length scales of oriented precipitates

The TEM images taken along the [100]-direction show a large number of θ'-Al_2Cu precipitates formed on the $(010)_\alpha$ and $(001)_\alpha$ planes, with a number density greater in the Al-4.0Cu alloy (Fig. 1b) than in the Al-2.5Cu alloy (Fig. 1a). The θ'-Al_2Cu precipitates have a plate-shaped morphology with coherent $(100)_{\theta'} \| (100)_{\alpha\text{-Al}}$ interfaces along the broad face and semi-coherent interfaces around the rim of the plates [46]. Previous reports stated that such structured θ'-Al_2Cu phase is non-shearable to dislocations under engineering tensile testing [47–50].

The characteristic length scales of precipitate arrays include their average diameter and spacing. The precipitate diameter is defined in Fig. 1c, and can be directly measured from the TEM images. Note that the θ'-Al_2Cu precipitates on $(100)_\alpha$ plane are invisible in the TEM images as a result of a low contrast [49], and all measurements are performed on the $(010)_\alpha$ and $(001)_\alpha$ precipitates. The measured precipitate number density is further corrected according to Ref. [49], which considers the equivalence of precipitation on the $\{100\}_\alpha$ planes. These measured precipitate diameters are broadly distributed (insets of Fig. 1a and b). However, it should be mentioned that TEM measurements inevitably exaggerate this scattering to some extent, as the TEM foils, with a thickness much smaller than the precipitate diameter, truncate the precipitates at a random position. Similarly, the real average precipitate diameter should be larger than the measured one, and can be corrected as follows [49]:

$$d_d = \frac{2}{\pi}\left(d_m - t_f + \sqrt{(d_m - t_f)^2 + 4\pi d_m t_f}\right) \quad (1)$$

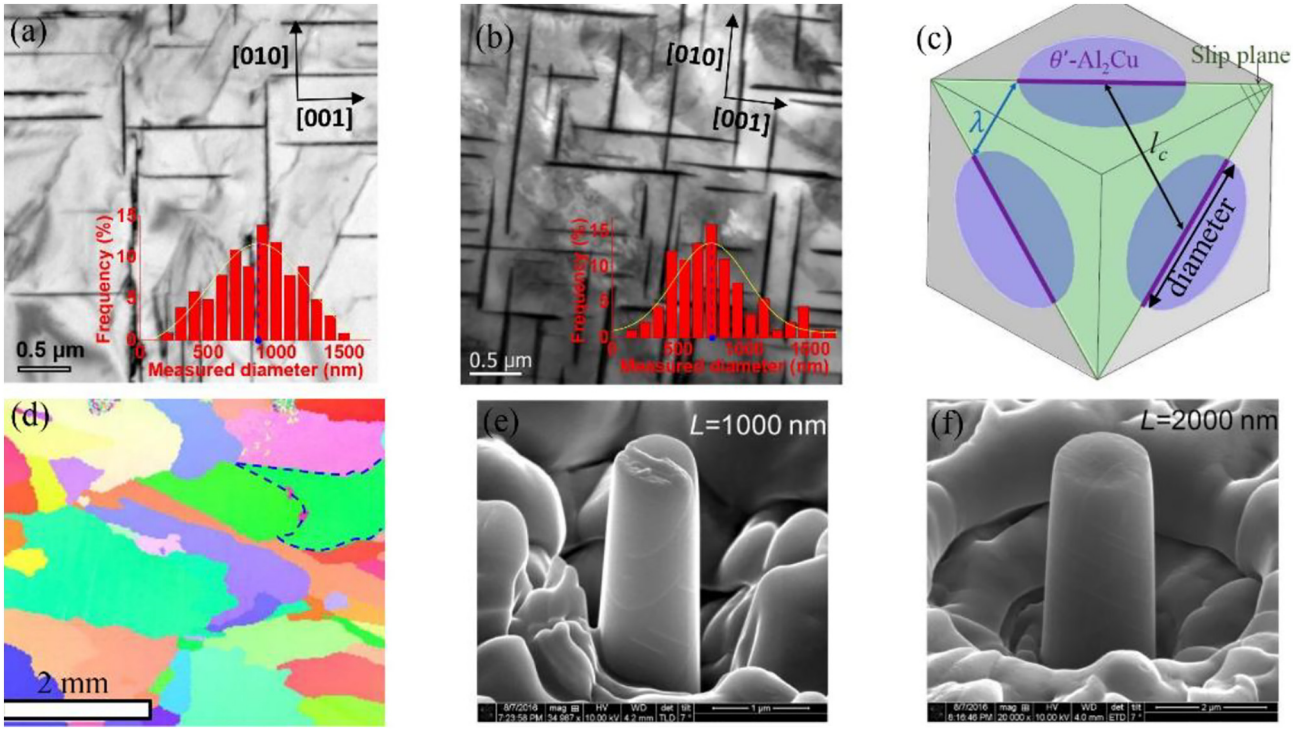

Fig. 1. The microstructure of tested materials and fabricated micro-pillars. (a) and (b) TEM images of Al-2.5Cu and Al-4.0Cu alloy respectively, taken along the [100]-direction. The insets in (a) and (b) show the distributions of measured precipitate diameters (c) Schematic diagram showing an ideal distribution of θ'-precipitates in the matrix. λ is the nearest spacing between precipitates, and l_c is the center-to-center distance between neighboring precipitates. (d) The EBSD mapping, where the [110]-orientated grain is marked by dot dash lines. (e) and (f) Typical images of Al-4.0Cu micro-pillars before compression, with 1000 and 2000 nm diameter respectively. The traces of intersections between the precipitates and the pillar surface can be observed.

where d_m and d_d are measured and real mean diameters, respectively, and t_f is the TEM foil thickness. The corrected average diameters d_d are comparable in Al-2.5Cu and Al-4.0Cu alloys (~ 1 μm, see Table 1).

To extract the average spacing between oriented precipitates, we consider an ideal distribution landscape of θ'-Al_2Cu precipitates [46,49], assuming that all plate-shaped precipitates are located at the center of each (100) surface of a cubic matrix volume (Fig. 1c). The average nearest spacing between precipitates, λ, is of particular importance, as it determines the critical stress for dislocations to overcome precipitates, hence the yield strength. For point-like disorder arrays ($\lambda \gg d_d$), this parameter λ solely characterizes the precipitate spacing. The situation is different here. In particular, one can keep λ unchanged while constructing a broader spacing inside the triangular array by enlarging the precipitate diameter d_d. Consequently, another important length scale of precipitate spacing, the center-to-center distance, l_c, should be introduced (Fig. 1c) [49]. It characterizes the dimension of the space surrounding by plate-like precipitates, and represents the distance that the dislocation segments can cross before encountering precipitates.

Using the experimentally measured precipitate parameters as summarized in Table 1, the spacing parameters λ and l_c can be determined from [49]:

$$\lambda = \frac{1.2669}{\sqrt{N_v d_d}} - \frac{\pi d_d}{8} - 1.061 t_d \tag{2}$$

$$l_c = \lambda + \frac{d_d}{2} + \frac{\sqrt{3}}{2} t_d \tag{3}$$

where N_v is the precipitate number density, and t_d the precipitate thickness. The values of λ and l_c are presented in Table 1.

3.2. Evaluation of pinning strength

The pinning strength, i.e., the resistance to dislocation motion arising from lattice resistance, forest dislocations, and quenched disorders, has been proved to be a critical parameter in controlling dislocation avalanches [17,36]. Following our previous work, we evaluate this pinning strength from the experimental measurements of yield strength, σ_y, of the bulk Al-2.5Cu and Al-4.0Cu polycrystalline alloys by tensile testing to avoid the external size effect on strength [17]. Because the studied bulk Al-Cu alloys have a texture-free, equiaxial grain structure, the

Table 1
Statistical and calculated results on the microstructure in the Al-Cu alloys.

Materials	Precipitate diameter, d_d (nm)	Precipitate thickness, t_d (nm)	Number Density, N_v (10^{18} m^{-3})	Volume fraction (%)	Pinning strength (MPa)	Nearest preci- pitate spacing λ (nm)	*Center-to-center spacing* l_c (nm)	Internal scale l (nm)
Al-2.5Cu	1190 (67)	13.0 (1.8)	1.69 (0.08)	2.44 (0.12)	35.0 (2.4)	412 (38)	1007 (82)	197 (14)
Al-4.0Cu	973 (85)	14.3 (2.9)	4.66 (0.30)	4.92 (0.38)	47.4 (2.1)	192 (17)	678 (47)	149 (7)

The values in the brackets are the measurement errors of microstructural parameters and bulk tension tests (pinning strength).

pinning strength can be estimated as follows [51]:

$$\tau_{pin}^{bulk} = \sigma_y/M - kL_g^{-1/2} \quad (4)$$

where M is the Taylor factor (3.06 for FCC), L_g the average grain size, and k the Hall-Petch constant (60 MPa·μm$^{1/2}$ [52]). The yield strength, σ_y, is measured as the 0.2% offset stress on the stress-strain curves of the bulk material. Note that the grain boundary strengthening is almost negligible compared with pinning strength, owing to the very large grain size in these alloys (~ 1 mm, Fig. 1d). The evaluated pinning strength of Al-2.5Cu alloy is ~35 MPa, smaller than ~47 MPa in Al-4.0Cu alloy (Table 1). Note that the so-evaluated τ_{pin}^{bulk} can only be used in micro-pillars with bulk-like dislocation-precipitate interaction, i.e., Orowan mechanism on {111}-plane, but becomes irrelevant if other interaction mechanisms take place.

4. Results

4.1. Plastic deformation curves of micro-pillars

Some representative engineering shear stress-strain curves are presented on Fig. 2 to highlight the external size and internal disorder effects, and their interplay, on plastic flow. At large external size $L \geq$ 3500 nm, both alloys deform in a smooth and continuous manner, similarly to their bulk counterparts, but with a higher yield strength (the stress at 0.2% plastic strain) (Fig. 2d). Decreasing the sample size to $L \approx$ 2000 nm intensifies plastic fluctuations, characterized by pronounced strain bursts and stress drops scattered on the stress-strain curves (Fig. 2c). The bursts appear smaller and rarer in Al-4.0Cu alloy than in Al-2.5Cu (Fig. 2c), indicating that the dense distribution of precipitates can tame intermittent plasticity effectively (Fig. 1a and b). Decreasing further the external size to L = 500 nm, strain bursts become more drastic, and of similar size in the two alloys (Fig. 2a). Besides these common features in the disorder-reinforced small samples [6,34,35], we find that that the size of load drops in 700 nm Al-2.5Cu micro-pillar (Fig. 2b) seems slightly smaller (less jerky) than, or similar with, what is observed for 1800 nm Al-2.5 Cu sample (Fig. 2c), in contradiction with the "smaller is wilder" effect. This anomalous phenomenon will be presented in more details in Sections 4.4.2 and 5.3.2.

4.2. Deformation morphology and its correlation with deformation curves

Representative SEM images of compressed Al-Cu micro-pillars with different sample sizes are shown on Fig. 3 and Fig. 4. Large specimens of both Al-2.5Cu and Al-4.0Cu alloys display numerous fine {111}-slip traces terminating inside the micro-pillars, and some of them intersecting with each other, as marked in Fig. 3a and c by white arrows (L = 4000 and 3500 nm respectively). These features can be linked to the inhibition of slip propagation across the entire sample by precipitates and dislocation short-range interactions, both of which are tightly link to mild plasticity [17,41]. Indeed, smooth deformation curves (Fig. 2d) are observed in these samples. Diminishing sample size leads to a gradual increase of plastic anisotropy, evidenced by the coarse slip bands observed in Fig. 3b and d (L = 1800 and 2000 nm respectively). This external size effect on plastic anisotropy and strain localization can be understood by a limited number of available sources lying on a few slip planes [9,10,53], and by the reduction of dislocation cross-slip, multiplication and storage before annihilation at free surface [13,54]. In this case, the long-range elastic interactions dominate the collective behavior of dislocations, resulting in the observed jerky stress-strain curves in Fig. 2c. The deformation curves of Al-4.0Cu alloy are less jerky than Al-2.5Cu alloy in Fig. 2c, consistent with a relatively less concentrated deformation and more slip bands when comparing Fig. 3d with Fig. 3b.

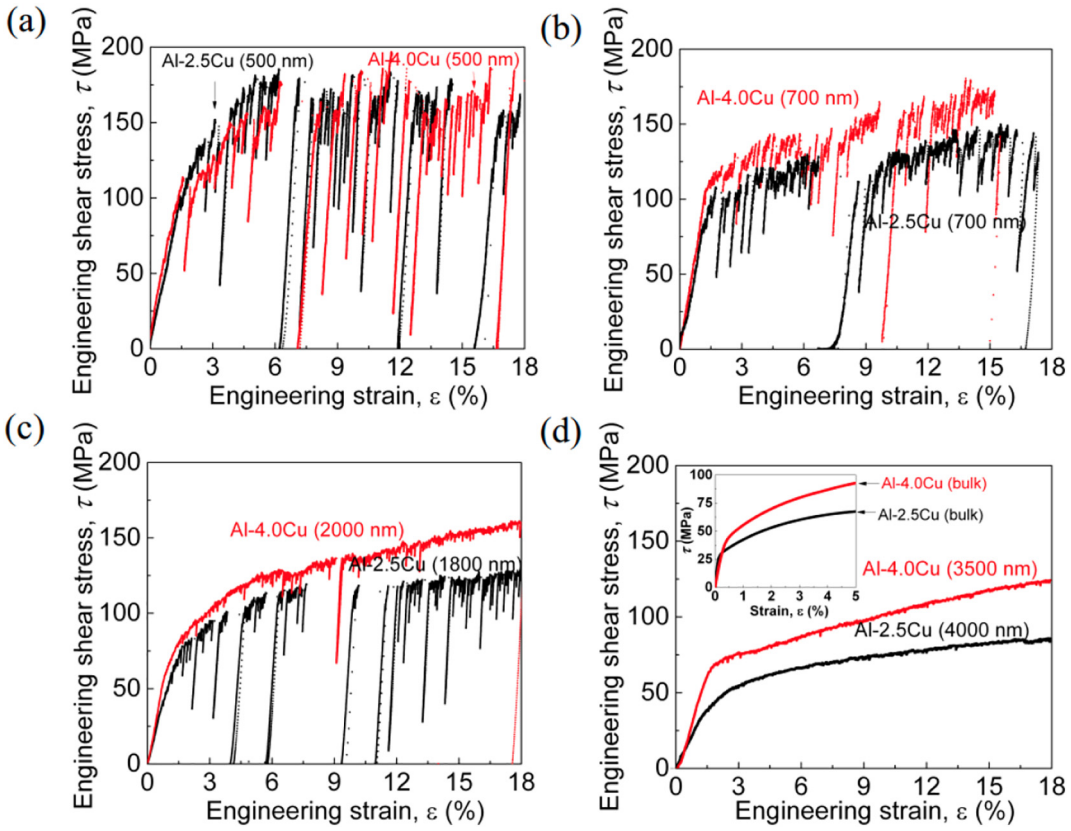

Fig. 2. Representative engineering shear stress-strain curves. Engineering shear stress-strain curves of Al-2.5Cu and Al-4.0Cu alloys with diameter of (a) 500 nm, (b) 700 nm, (c) 1800 and 2000 nm respectively, and (d) 4000 and 3500 nm respectively. The shear stress τ is calculated by multiplying the compression stress with Schmid factor on {111}-plane. The shear stress-strain curves for bulk polycrystalline samples are given in the inset of (d).

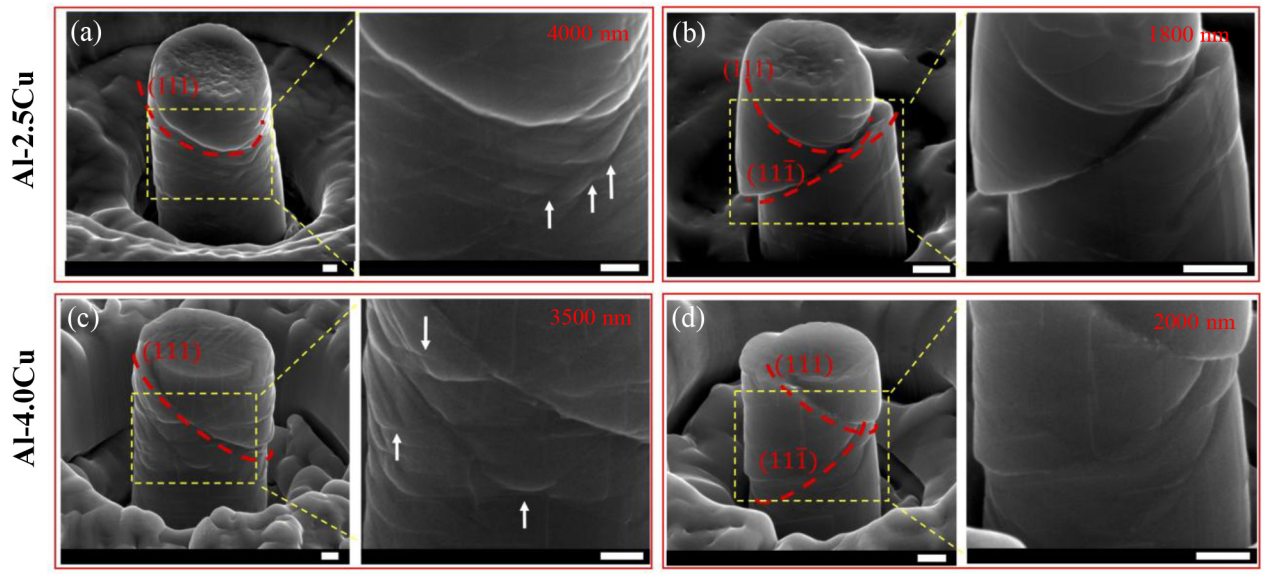

Fig. 3. Representative SEM images showing the deformation morphology of Al-Cu alloys after 18% compression strain. Al-2.5Cu micro-pillars with diameters $L = 4000$ nm (a), 1800 nm (b), and Al-4.0Cu micro-pillars with diameters $L = 3500$ nm (c), 2000 nm (d). The zoom views of the images show the slip traces more clearly. The white arrows in (a) and (b) mark the intersections of slip traces. The Miller indices of coarse slip traces are marked according to the sketches shown in Fig. 4. All the scale bars represent 500 nm.

On the other hand, when the external size matched the precipitate diameter, $L/d_d \approx 1$, we observed in some micro-pillars highly distorted deformation morphologies, showing not only traditional {111}-slip traces, but also slip traces along non-close-packed planes (Fig. 4a and d). This unexpected phenomenon was only observed over a limited diameter range, $700 \le L \le 1000$ nm for Al-2.5Cu and $500 \le L \le 1000$ nm for Al-4.0Cu alloy, and disappeared upon further decreasing the sample size (Fig. 4b). The trace analysis (Fig. 4c and f) suggests that these non-trivial slip traces are caused by slip along {100}-planes. According to our knowledge, {111}-slip has been considered as the only slip mode at room temperature in pure Al and Al alloys, even in the nano-sized samples under an external stress approaching the theoretical strength [12,55]. In a recent work [56], we show that this {100}-slip occurs along the coherent θ'-Al_2Cu precipitate/α-Al matrix interface, and we analyze the mechanisms giving rise to this unusual interfacial slip. Here we focus on the consequences of this slip mode in terms of mechanical behavior and plastic intermittency.

To illustrate the role of {100}-slip on the mechanical behavior, we present two compressed Al-4.0Cu micro-pillars of the same size ($L =$ 1000 nm) in Fig. 4d and e: the first one displays a distorted morphology and obvious {100}-slip traces (Fig. 4d), while the other one exhibits coarse slip traces along {111}-plane (Fig. 4e). The corresponding engineering stress-strain curves are given in Fig. 4g and h. In micro-pillars with {100}-slip traces, the initial jerky behavior progressively vanishes with increasing strain while some "apparent strain hardening" (engineering stress increase with strain) is observed, in strong contrast with micro-pillars showing {111}-slip only. As true stress and strain cannot be properly estimated in micro-pillar compression [57], the intrinsic hardening is actually inaccessible. A larger "apparent hardening rate" in {100}-slip samples may stem from an enhanced dislocation storage ability, or from a different deformation pattern giving a distorted morphology. In Section 4.4, we will quantify the differences between these two slip modes in terms of wildness and scaling exponent.

4.3. Strength of micro-pillars

In micro-pillar compression, the strength of samples can be characterized by the flow stress at a given strain value, typically between 2% and 10% [3,4,58], or, possibly, by the stress at the first detected strain burst [59]. However, our micro-pillars cover the wild and mild regimes. In the mild regime, such as the Al-2.5Cu micro-pillars with 4000 nm diameter (Fig. 2d), strain bursts are, by definition of wildness, rare and limited in size. In this case, the first detected burst is observed for large strains, far beyond the elastic-plastic transition. In other words, a yield criterion based on the detection of the 1st burst would depend on the degree of wildness itself. To minimize the effect of "apparent strain hardening", as well as problems in the estimation of stress and strain at large deformation [57], we simply use the *engineering* yield criterion of the stress at 0.2% plastic strain by following the works in Ref. [60–62].

Fig. 5a shows the critical resolved shear stress τ_{yield} on {111}-plane, calculated from this 0.2% offset stress multiplied by the Schmid factor (0.408 for [110]-orientation), as a function of external size L. The data for pure Al is taken from our earlier work [17]. On Fig. 5a, the stronger materials exhibit a weaker size effect, consistent with an enhanced role of disorder (i.e., external-size independent) on strength [34,35,63]. It should be noticed that the differences of strength between Al-Cu alloys and pure Al counterparts vanish as decreasing the sample size to 500 nm. This is shown on Fig. 5b where the strength gain, $\Delta\tau_{yield} = \Delta\tau_{yield}^{Al-Cu} - \Delta\tau_{yield}^{Al}$, is represented as a function of the external size L. $\Delta\tau_{yield}$ remains almost constant at large L, but decreases towards zero at a critical diameter. Such transition has been investigated in irradiated Cu micro-pillars [64], and attributed to a vanishing of dislocation-disorder interactions in small samples. A detailed analysis of strength is presented in Section 5.2.

4.4. Statistics of fluctuations

4.4.1. Methodology

Determining the nature and origin of stochastic fluctuations in plasticity first relies on the quantification of their statistical properties [17]. Recently, we proposed a data mining procedure, based on the definition of an "avalanche" as a plastic process characterized by a dissipation rate much greater than the imposed loading rate, allowing to extract avalanches from smooth flow through an objectively determined threshold (see Section 4.1 of Ref. [17] for details). The size of a burst is quantified by the axial plastic displacement released as a result of dislocation motion: $X = D_e - D_s + (F_s - F_e)/K_p$, where D_s, F_s, D_e and F_e are the displacement and force when a detected displacement jump starts and ends, respectively, and K_p is the stiffness of the sample [17]. Theoretically, X scales with the cumulative area swept by the dislocations involved in

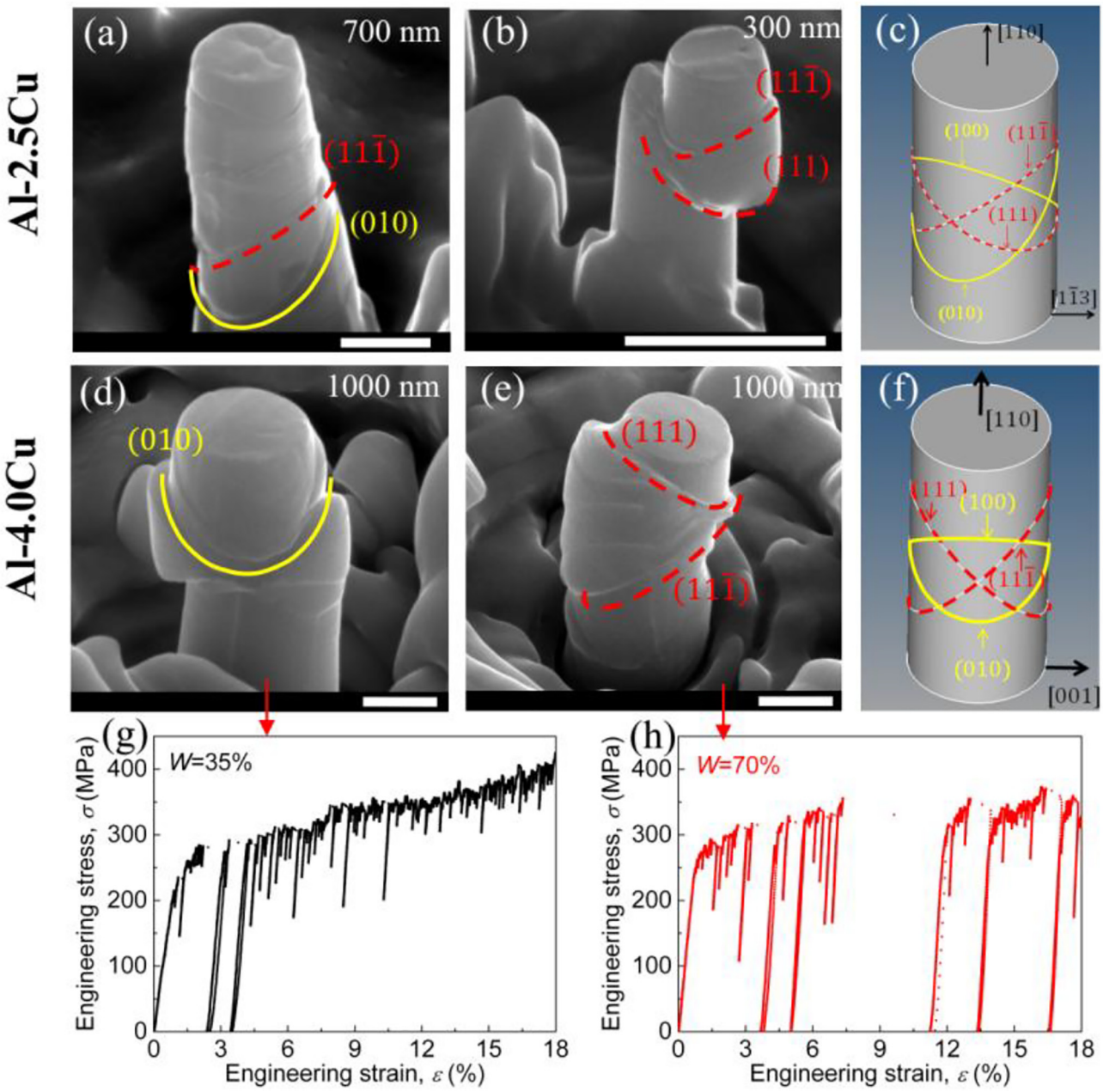

Fig. 4. Comparisons of deformation morphologies and engineering stress-strain curves for micro-pillars with {111}-slip and {111} + {100}-slip. SEM images of Al-2.5Cu micro-pillars with diameters of $L = 700$ nm (a) and 300 nm (b), and Al-4.0Cu micro-pillars with a diameter of $L = 1000$ nm (d) and (e). Sketches in (c) and (f) represent the shapes of slip traces corresponding to the observed directions in Al-2.5Cu and Al-4.0Cu alloys respectively. The Miller indices of coarse slip traces in SEM images are marked according to (c) and (f). (g) and (h) are the corresponding stress-strain curves to show the differences of mechanical response for micro-pillars of the same size with (d) and without (e) {100}-slip traces. All the scale bars represent 500 nm.

the avalanche, ΔA, between the two elastic states $((D_s,F_s)$ and $(D_e,F_e))$: $X \sim b(\Delta A/A)$ [65], where A is the area of the sample cross section. Once these bursts are extracted, a robust maximum likelihood methodology [66] is used to estimate the lower bond X_{min} of power law scaling $P(X) \sim X^{-\kappa}$, and the scaling exponent κ. The fraction of plastic deformation accommodated through power law distributed bursts $(X > X_{min})$ defines the wildness W. More details can be found in our recent work (Section 4.1 and SM of Ref. [17]).

4.4.2. Effects of external size and disorder on wildness

The statistical results of plastic fluctuations as a function of micro-pillar diameter L are presented in Fig. 6, in terms of wildness W and scaling exponent κ. The trend of "dirtier is milder" is recovered for these two Al-Cu alloys, with a milder deformation (small W) in Al-4.0Cu compared with Al-2.5Cu micro-pillars (Fig. 6a), which we interpret as a reduction of the "mechanical temperature" of the system when increasing the pinning strength of the obstacles [17,41]. More specifically, the pinning effect acting on dislocations frustrates the long-range elastic mutual interactions [36] and facilitates short-range reactions as well as deformation isotropy (see Section 4.2), thus driving plasticity towards a mild regime [17]. However, another typical effect of sub-μm plasticity, expressed as "smaller is wilder", is broken down at an intermediate diameter range: the wildness of the micro-pillars exhibiting {100}-slip traces drop from the general trend (Fig. 6a), thus confirming the qualitative statement in Section 4.1. This anomalous behavior is interesting, as it may suggest a methodology to mitigate the detrimental effect of "smaller is wilder" in NEMS by introducing precipitates with a size comparable to device dimensions.

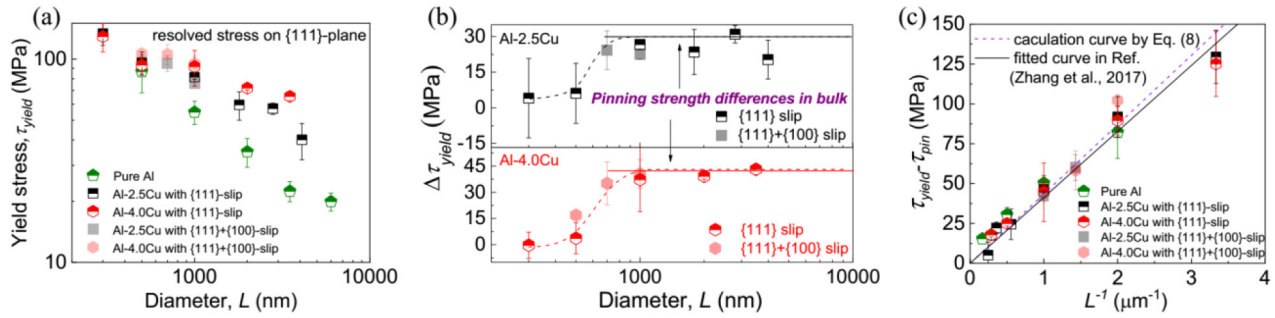

Fig. 5. External size dependent strength. (a) Experimental results of the L-dependent yield stress (0.2% offset stress multiplied by Schmid factor) for Al-Cu alloys on {111}-plane, together with the data of pure Al taken from Ref. [17]. (b) Strength increment in Al-Cu alloys relatively to pure Al as a function of L. Below a critical diameter, the strengthening effect of precipitates vanishes. (c) The effective shear stress to activate truncated dislocation source, $\tau_{yield} - \tau_{pin}$, as a function of external size. A universal relation $\tau_{yield} - \tau_{pin}$~$1/L$ can be identified. The black solid line is taken from Fig. 11 of Ref. [17] and the purple dash line is calculated by Eq. (8). Here τ_{pin} is the pinning strength to dislocation motion, originating from lattice resistance, forest dislocations and precipitates. (For interpretation of the references to color in this figure legend, the reader is referred to the web version of this article.)

Besides the wildness W, the distributions of displacement burst sizes (compiled over the entire loading process) are also given in Fig. 6. For small samples (e.g., $L = 500$ nm on Fig. 6c and d), the exponents κ are slightly above the mean field theory [29,67] and DDD simulations [19,68,69] prediction, $\kappa \sim 1.5$, corresponding to essentially power-law distributed fluctuations and a maximum wildness ($W \to 1$) , while κ is observed to increase significantly upon increasing the sample size, in association with a decreasing wildness. We noted above that micro-pillars with {100}-slip traces exhibited a lower wildness than the ones with {111}-slip only. This anomalous behavior is expressed also in term of scaling exponent, showing a larger κ for the 700 nm Al-2.5Cu micro-pillars with {100}-slip than for the 1000 and 1800 nm micro-pillars of the same material with {111}-slip only (Fig. 6c). This association between larger scaling exponents κ and {100}-slip is also observed for Al-4.0Cu micro-pillars (Fig. 6d).

We have shown previously from tests on pure Al and nm-sized disorder-reinforced Al alloys [17] that the combined effects of external size and disorder on plastic intermittency manifested themselves through a unique (material independent) mapping between the power law exponent and wildness, $W(\kappa)$ (see the purple points in Fig. 6b). Here we show that this "universal" relation holds for the μm-sized precipitate reinforced Al-Cu alloys (Fig. 6b). Quite remarkably, it even holds for the micro-pillars with {100}-slip traces where different deformation mechanisms are believed to operate (solid semi-transparent symbols in Fig. 6b).

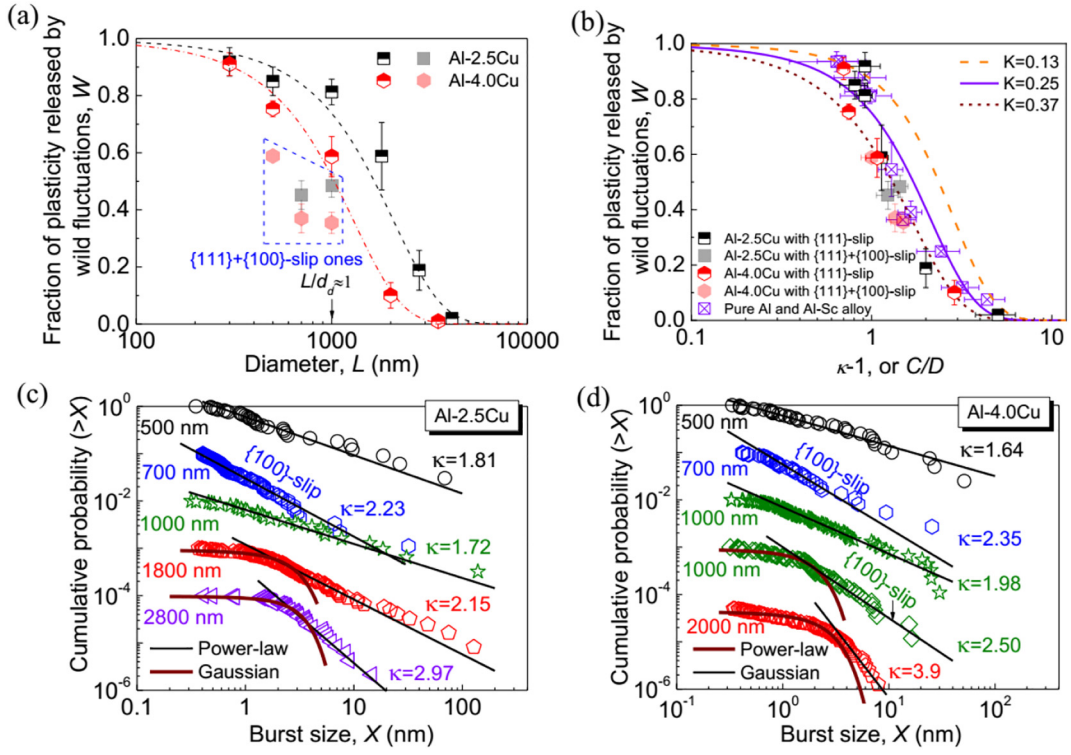

Fig. 6. Statistics of intermittent plasticity. (a) The external size dependent wildness of Al-Cu alloys. The solid semi-transparent symbols represent the micro-pillars showing {111} + {100}-slip traces. (b) The universal relation between wildness W and power law exponent κ-1. The data for pure Al and Al-Sc alloys are taken from Ref. [17]. (c) and (d) Typical strain burst distributions in Al-2.5Cu and Al-4.0Cu alloys respectively, where the samples showing {100}-slip traces are labelled. The burst distributions of samples with 1000 nm diameter in (d) correspond to the micro-pillars of Fig. 4d and e.

5. Discussion

5.1. Length scales vs regimes of plastic deformation

The dependence of the mechanisms of plasticity on external size L in single crystals can be speculated from a rough length scale analysis, comparing L with the microstructural length scales of dislocation networks, l_{dn}, and disorder arrays, l_{da}. For our case, the characteristic length scale of disorder arrays l_{da} includes the diameter of plate-like precipitate, d_d, as well as the spacing between precipitates (λ and l_c, see Section 3.1).

In the upper limit, $L \gg l_{dn}, l_{da}$, the samples are large enough to be representative volume elements (RVE) for the disorder and the dislocation network of the corresponding bulk alloys. Hence, we expect a plastic behavior controlled by the internal structure and characterized by an external size independent strength and mild deformation. The strengthening mechanisms of plate-like precipitates in this regime have been recently studied by micro-pillar compression [70]. In the lower limit, $L \ll l_{dn}, l_{da}$, the samples actually degrade to their pure microcrystal counterparts, with an absence of dislocation-disorder interactions before dislocation annihilation at free surfaces (schematically shown on Fig. 7c). This is exactly the case in our small samples, as shown by a vanishing strength difference between Al—Cu alloys and pure Al when $L \leq 500$ nm (Fig. 5b). Between these two extreme cases, a complex regime emerges from a combination of external size and internal disorder effects. The case $l_{da} \ll L < l_{dn}$, where the sample can only be considered as a RVE for the disorders (not for the dislocation network), was considered in our previous work [17]. In this regime, the sample strength can be considered as a superposition of disorder strengthening and dislocation activation/nucleation stress [4,71], and the plastic fluctuations are controlled by the competition between the external size L and an internal length scale $l = Gb/\tau_{pin}$ [17], where G is the shear modulus, b is the magnitude of Burgers vector, and τ_{pin} is the pinning strength to dislocation motion, originating in alloys mainly from disorder arrays.

However, in case of $l_{da} \sim L < l_{dn}$, a strong interference between the external size and the disorder related length scales is expected, as for the present Al-Cu alloys. Detailed investigations in this regime are still lacking. We can speculate that the dislocations can bypass precipitates when $L/d_d > 1$ (Fig. 7a), but would pile-up against the precipitate/matrix interface if the precipitates cut off the entire micro-pillar (Fig. 7b). However, beyond this simple reasoning, to what extent the mechanical properties in this regime fit into the previous frameworks, and what are the plastic mechanisms specific to these Al-Cu alloys, remain open questions. In what follows, we will first extract the features common to all alloys and length scales, and then discuss the specific plastic mechanisms of the Al-Cu alloys in the regime $l_{da} \sim L < l_{dn}$.

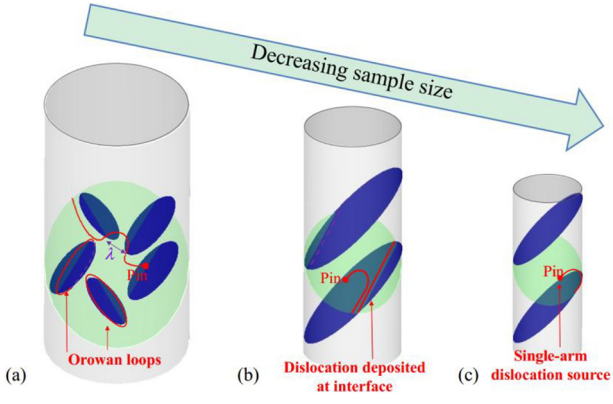

Fig. 7. Deformation mechanisms of Al-Cu micro-pillars. (a) For large sample sizes, the precipitates are surrounded by the Al-matrix, thus the mobile dislocations can bypass precipitates through bulk-like Orowan mechanism. (b) For samples of intermediate size, the plate-like precipitates cut off the entire micro-pillar, forming a multilayer-like microstructure. In this case, the dislocations pile-up against the precipitate/matrix interface instead of bypassing precipitates. (c) For small samples, dislocations can run across the micro-pillar within the interval between two precipitates, without interacting with them.

5.2. Universal features in plastic fluctuations and yielding

5.2.1. Dislocation-disorder interactions

Analyzing the strength of Al-Cu micro-pillars can shed light on the dislocation-disorder interactions that play a crucial role in plastic avalanches. For μm to sub-μm pillars, their strength has been considered to be a superposition of the pinning strength of disorder and the activation stress of the weakest single-arm dislocation source (SAS) [10,72–74]:

$$\tau_{yield} = \tau_{pin} + \frac{\alpha G b}{l_s(\rho, L)} \tag{5}$$

where l_s is the length of the weakest SAS, and α is a geometrical constant of order of unity. To estimate the pinning strength τ_{pin} in micro-pillars, we compare on Fig. 5b the strength difference between Al-Cu and pure Al micro-pillars, $\Delta\tau_{yield}$, with the corresponding difference for bulk samples, $\Delta\tau_{bulk}$. From Eq. (5), we expect $\Delta\tau_{yield} = \tau_{yield}^{Al-Cu} - \tau_{yield}^{Al} = \tau_{pin}^{Al-Cu} - \tau_{pin}^{Al} = \Delta\tau_{bulk}$, which is recovered for sample sizes $L \geq 700$ nm. This means that the strengthening mechanisms acting in these samples are essentially unchanged compared with bulk samples, i.e., τ_{pin} can be safely estimated from Eq. (4). On the other hand, when $L \leq 500$ nm, as shown in Section 4.3 and discussed above, dislocation-precipitate interactions vanish and the samples behave as pure Al. Within this diameter range, we can therefore consider $\tau_{pin}^{Al-Cu} = \tau_{pin}^{bulk\ Al}$.

5.2.2. Wild-to-mild transition

The typical effect of sub-μm, expressed as "smaller is wilder", is quantified in Fig. 6a. The enhanced role of the free surface as decreasing L reduces the possibility of mutual dislocation reactions, leading to an absence of self-induced dislocation microstructure that suppresses plastic instability in large samples [41]. In addition, the increasing external stress can break the dislocation entanglements, resulting in pronounced dislocation avalanches (see the model and the experimental relations between burst size and external stress in [17,75,76]). The wild-to-mild transition can be shifted to small size by introducing disorders.

In our previous work [17], we translated the pinning strength of disorders into a characteristic length scale $l = Gb/\tau_{pin}$ characterizing the competition between disorder-dislocation interactions and long-range elastic mutual interactions between dislocations. l represents a distance at which the long-range elastic stress associated with a dislocation becomes similar to the pinning stress of disorder. This way, we found that a single non-dimensional parameter $R = L/l$ unifies the transition from wild to mild fluctuations for different materials. In the present study, using the τ_{pin} values for micro-pillars as explained in the above section, we are still able to gather the wildness values of {111}-slip Al-2.5Cu and Al-4.0Cu samples onto a single curve (Fig. 8a), and the overall shape (sigmoidal) of the wild-to-mild transition remains unchanged. This suggests that the main features of the wild-to-mild transition in the Al-Cu samples can still be captured by our previous framework, meaning that the effect of pinning strength on the long-range elastic interactions between dislocations remains a major factor on preventing intermittency in the Al-Cu alloys.

Since we considered above only the slip resistance on {111}-planes, it is not surprising to observe that {100}-slip micro-pillars deviate from the $W(R)$ curve of Al-Cu alloys (Fig. 8b). Introducing the Peierls stress of the dislocation glide along the coherent precipitate/matrix interface, calculated to be ~ 80 MPa [56], into the relation $l = Gb/\tau_{pin}$ to estimate R, the data points of {111} + {100}-slip samples move onto the sigmoidal line (Fig. 8b), indicating a contribution from this non-trivial slip mode to the inhibition of plastic fluctuations.

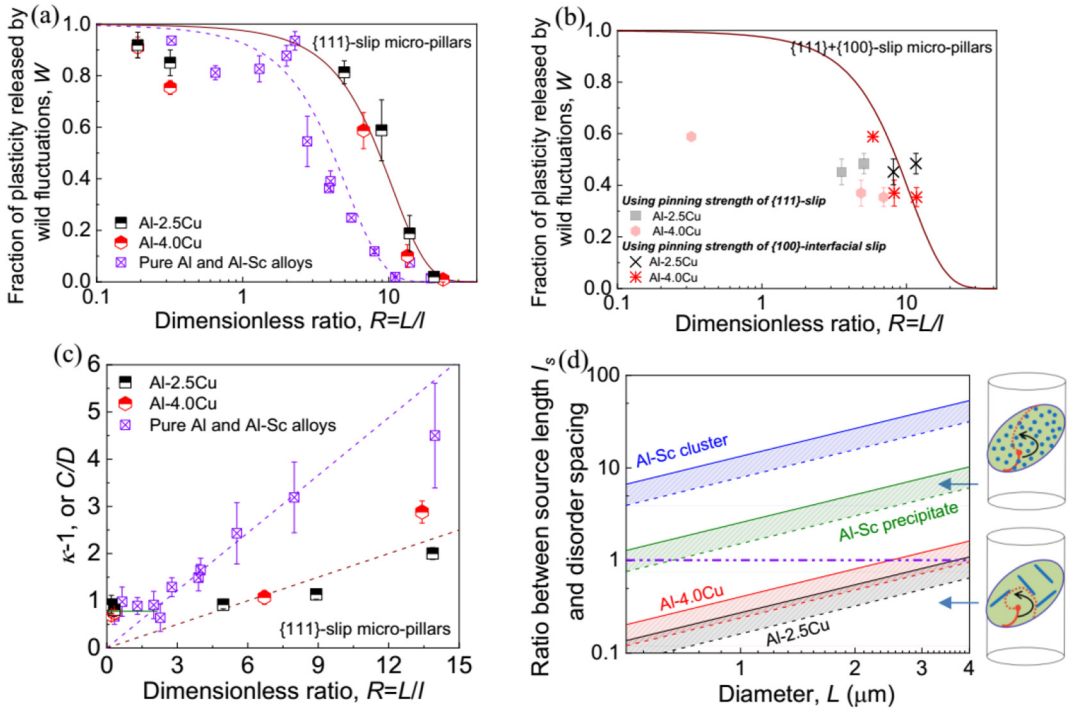

Fig. 8. Statistics of intermittent plasticity as a function of R and dislocation-disorder interaction map. (a) The wildness W of {111}-slip micro-pillars as a function of non-dimensional ratio R. The sigmoidal curves are calculated from the model, using the universal relation $W(C/D)$ in Eq. (6) and the linear relation C/D~L/l in (c). (b) The wildness W of {111} + {100}-slip micro-pillars as a function of R. The pinning strength of dislocations slipping along both {111}-plane of matrix and {100}-interface are used to estimate R. The solid curve is as the same as the one in (a). (c) The relation between the power law exponent $C/D = \kappa - 1$ and R for {111}-slip micro-pillars. (d) The ratio between the length of dislocation sources l_s and the disorder spacing (λ for solution clusters and nm-sized precipitates, and l_c for μm-sized precipitates) as a function of external size L. Both initial and stable dislocation sources are considered, giving the ratio range in (d). The sketches in (d) are to illustrate the differences of pinning landscapes in the two regimes. The blue objects in the sketches represent the cross-section of precipitates on the {111} slip plane. For Al-Cu alloys, the plate-shaped precipitates will form a triangular array on slip planes. The data of pure Al and Al-Sc alloys are taken for Ref. [17]. (For interpretation of the references to color in this figure legend, the reader is referred to the web version of this article.)

5.2.3. The universal relation $W(\kappa)$

Instead of mean-field theory arguing for a universal landscape of intermittent plasticity [29], it has been revealed that the associated statistical properties are material- and size-dependent, with varying scaling exponent κ and wildness W [17,41,77–80]. Note that the loading method in these experiments remain the same, and the varying κ should not be an effect of machine stiffness analyzed in [81,82]. On the other hand, we found that the relationship between these two variables, $W(\kappa)$, in pure Al and nano-sized disorder reinforced Al alloys, is "universal" (material-independent) [17]. In the present study, we extend this relation to the Al-Cu alloys containing μm-sized precipitates (Fig. 6b). This is quite remarkable, as it suggests that this relation not only holds for materials containing large-sized precipitates, but also for samples showing totally different deformation mechanisms ({100}-slip and distorted morphology). In other words, this indicates that the $W(\kappa)$ relationship may be truly universal, even does not depend on microscopic plastic mechanisms.

This is in full agreement with our previously proposed stochastic model for the evolution of mobile dislocation density ρ_m that gives [17,41]:

$$W = 1 - \frac{\Gamma\left(\frac{C}{D}, log\left(\frac{1}{K}\right)\right)}{\Gamma\left(\frac{C}{D}, 0\right)} \tag{6}$$

where C is the rate of mutual annihilation/immobilization of the dislocation pairs; D is the intensity of a multiplicative mechanical noise that describes fluctuations experienced by a representative volume due to interactions with the rest of the system, which can also be seen as the mechanical temperature of the system; $\Gamma(z,x) = \int_x^\infty t^{z-1}e^{-t}dt$, and K is a parameter setting a threshold to distinguish the power law tail in the model. In this model, the ratio C/D is linked to the power law exponent, $C/D = \kappa - 1$ [41]. Although $C/D = \kappa - 1$ and W depend on external size and plastic mechanisms, Eq. (6) predicts that W depends solely on C/D, as shown on Fig. 6b, whatever the material, and is independent of microscopic plastic mechanisms. Note that Eq. (6) weekly depend on parameter K [17]. Based on the universal relation $W(C/D)$ in Eq. (6) and the scaling $C/D \sim L/l$ in {111}-slip Al—Cu alloys identified on Fig. 8c, the wild-to-mild transition on Fig. 8a can be recovered.

5.2.4. Yield stress scaling

As discussed in Section 5.2.1, micro-pillar yield stress is considered to be a superposition of the pinning strength of disorder and the activation stress of the weakest SAS, $\tau_{yield} = \tau_{pin} + \frac{\alpha G b}{l_s(\rho, L)}$ (Eq. (5)), where l_s is a function of the dislocation density ρ and external size L [10,61,83,84]. An expression for the length of the weakest SAS at the *onset* of plastic flow was proposed from 3D discrete dislocation dynamic (DDD) simulations of pure single crystals [83], for $\rho L < 10^7$ m^{-1}, i.e., when considering an initial dislocation density of order 10^{12} m^{-2}, for sample sizes typically below few μm:

$$l_s = \frac{bL\sqrt{\rho}}{\eta} \tag{7}$$

where the parameter $\eta = 1.76 \times 10^{-3}$ is a dimensionless constant. Combining Eqs. (5) and (7) we get:

$$\tau_{yield} - \tau_{pin} = \frac{\alpha G \eta}{\sqrt{\rho}} \frac{1}{L} \tag{8}$$

This scaling $\tau_{yield} - \tau_{pin} \sim 1/L$ is consistent with a re-evaluation of a large set of published experimental data [63], and has been verified in

our pure Al and Al alloys in Ref. [17]. Using the pinning strengths obtained in Section 5.2.1, a remarkable convergence of data, including pure Al and Al alloys previously studied [17] as well as the present results, towards a single master curve is obtained (Fig. 5c). Taking an initial dislocation density of $\rho = 10^{12}$ m^{-2} for well annealed samples and $\alpha = 1$, Eq. (8) fits the experimental data very well (dashed line on Fig. 5c).

The universality of Eq. (8), for pure Al to Al alloys, indicates that $l_s(\rho,L)$ in Eq. (7) can be extended to Al alloys at plastic yield, i.e., the $l_s(\rho,L)$ at the *onset of plastic flow* only depends on dislocation density and sample size, not on disorder. Moreover, on Fig. 5c we only considered the resolved shear stress on {111}-planes, even for samples with {111} + {100} slip traces. Still, these {111} + {100}-slip samples fit the universal relation Eq. (8), indicating that the yield stress in these samples should be essentially controlled by {111}-slip, in contrast with a wildness controlled (reduced) by {100}-slip (see Section 4.4.2). Indeed, if the initial stage of plasticity is controlled by the weakest slip system, upon increasing the strain further, other mechanisms such as {100}-slip take place and reduce the wildness. This is consistent with the observation that, in these samples, the jerkiness of stress-strain curves decreases with increasing strain (Fig. 4g).

5.3. Specific mechanisms in Al—Cu micro-pillars

5.3.1. Disorder effect on taming intermittency

In Section 5.2.2, translating the pinning strength into an internal length scale, $l = Gb/\tau_{pin}$, we found that the dimensionless ratio $R = L/l$ unifies the wild-to-mild transitions of Al-2.5Cu and Al-4.0Cu alloys. However, compared with the previous Al alloys containing nano-sized disorders [17] (purple points on Fig. 8a), the sigmoidal transition is shifted for the present alloys towards larger *R*-values. Actually, for materials with strong lattice resistance or dense nano-sized disorders, the pinning effect works on a scale of atomic distance, or of disorder spacing, much smaller than the average length of mobile dislocation segments. In this case, the mobile dislocation segments must overcome this pinning effect to move. However, this mean-field pinning picture is questionable for Al-Cu micro-pillars, where the precipitates spacing is commensurate with the sample size, hence with the length of dislocation segments. To explore this situation, we take the SAS length l_s as a characteristic length of mobile dislocation segments, considering that plasticity is largely associated with the activation and shutdown of SAS in the source-truncation regime [9], and compare l_s with the precipitate spacing determined in Section 3.1.

Eq. (7) gives l_s at the onset of plastic flow. This source length should evolve with deformation. Cui et.al [85] gives an expression of the stable SAS length at the flow stage, for micro-pillars with a typical initial dislocation density obtained in FIB-milled specimens:

$$l_s = \frac{L}{4\cos^2(\beta/2)} \tag{9}$$

where β is the angle between the normal to the slip plane and the loading axis. This expression gives $l_s = 0.317\,L$ for the [100]-oriented micro-pillars, which has been validated by the statistic measurements of l_s in their DDD simulations, and by the work of Ryu et al. [84]. For the [110]-oriented micro-pillars of the present study, Eq. (9) gives $l_s = 0.254\,L$. The characteristic length of dislocation segments, both at the yield (Eq. (7)) and flowing (Eq. (9)) stages, were compared with the largest length scale characterizing precipitate spacing, which is l_c for plate-like precipitates, and λ for nanometer sized disorder reinforced alloys (see Section 3.1). Fig. 8d shows that, in contrast with the Al alloys micro-pillars of Ref. [17], the source lengths in the present Al-Cu micro-pillars are smaller than the precipitate spacing, $l_s/l_c < 1$. This clearly means that the weakest dislocation sources can be activated and then move inside the plate-like precipitate array before getting pinned (see the sketch for Al-Cu alloy in Fig. 8d). This breakdown of the mean-field pinning picture, a typical feature of alloys containing plate-like precipitates of size comparable with the external size, seems to not affect the *global* properties, such as yield strength scaling (Fig. 5c). However, it makes the dislocation motion sensitive to small stress perturbations at *micro-scale* before getting pinned. In our model words, it increases the *local* "mechanical temperature" of the system [17,41], leading to wilder fluctuations when comparing with the mean-field pinning case (upper sketch on Fig. 8d) with a same *R*.

5.3.2. Special mechanisms related to penetrating precipitate

As schematically shown in Fig. 7b, when the external size *L* becomes comparable with the precipitate diameter d_d, the precipitates can cut off the micro-pillar, forming a multilayers-like structure. This structure, which can be seen in the TEM image of the longitudinal section of a micro-pillar with {100}-slip traces (Fig. 9a), prevents dislocations to bypass the obstacles. Consequently, dense dislocation networks are observed near the precipitates as a result of dislocation pile-ups (Fig. 9b). This strong inhibition of slip can enhance the strain isotropy (see the in-situ compression below) and dislocation short-range interactions, which are associated with mild deformation [17]. Moreover, the straight dislocations in Fig. 9c and d, with lengths much larger than the thickness of the foil, necessarily lie within the TEM foil plane (100). These (100)-dislocations with zero Schmid factor are most likely to be the geometrically necessary dislocations (GNDs) generated to accommodate the strain gradient near the penetrating plate-like precipitate. These GNDs can serve as obstacles to mobile dislocations, hence inhibiting the plastic intermittency ever further. Based on these understandings, as well as the observed {100}-slip traces, we conclude that the sharp decrease of wildness in the micro-pillars containing penetrating θ'-Al_2Cu plate-like precipitates (Fig. 6a) should be a result of different factors, including the high slip resistance of abnormal {100}-interfacial slip [56], the enhanced strain isotropy and the inhibition effect from the generated GNDs.

5.3.3. Taming intermittency by using penetrating precipitates

We showed above that plastic slip along {100}-planes and the shearing of precipitates due to dislocation pile-ups are the main deformation mechanisms when precipitates cut off the micro-pillars. In order to show the effectiveness of this special configuration on suppressing plastic intermittency, two [110]-oriented micro-pillars with square cross-section (~220 × 220 nm), one containing precipitates and the other not, were fabricated at the edge of an Al-2.5Cu foil and compressed in-situ under TEM (Fig. 10). For the sample without precipitate, the deformation behavior was, as expected, similar to that of pure Al samples with a similar size [17,42], with plastic strain highly localized on a single slip plane (Fig. 10b and c). The generated dislocations quickly slipped across the sample in an intermittent way, and wild deformation was observed (Fig. 10d). In contract, in the micro-pillar containing penetrating precipitates (Fig. 10e), the dislocations piled-up against the θ'-precipitate (marked in Fig. 10f) upon gradually increasing the displacement. The configuration of dislocation pile-ups is similar to the TEM observation of Fig. 9b. Upon deforming the micro-pillar further, these pile-up dislocations sheared the θ'-precipitate, resulting in a broadening of the precipitate (Fig. 10g). The {100}-slip steps can also be identified at the tip of the θ'-precipitate (black arrows in Fig. 10g). These mechanisms tame intermittency and prevent the development of strain localization, inducing a homogenous diameter expansion (marked in Fig. 10g) and mild plasticity (Fig. 10h). Moreover, the penetrating θ'-Al_2Cu plate-like precipitate can limit the space for collective dislocation motions, hence inhibiting the intermittent plasticity. These in-situ compression tests confirmed that the introduction of penetrating precipitates promotes strain homogeneity while taming plastic intermittency effectively.

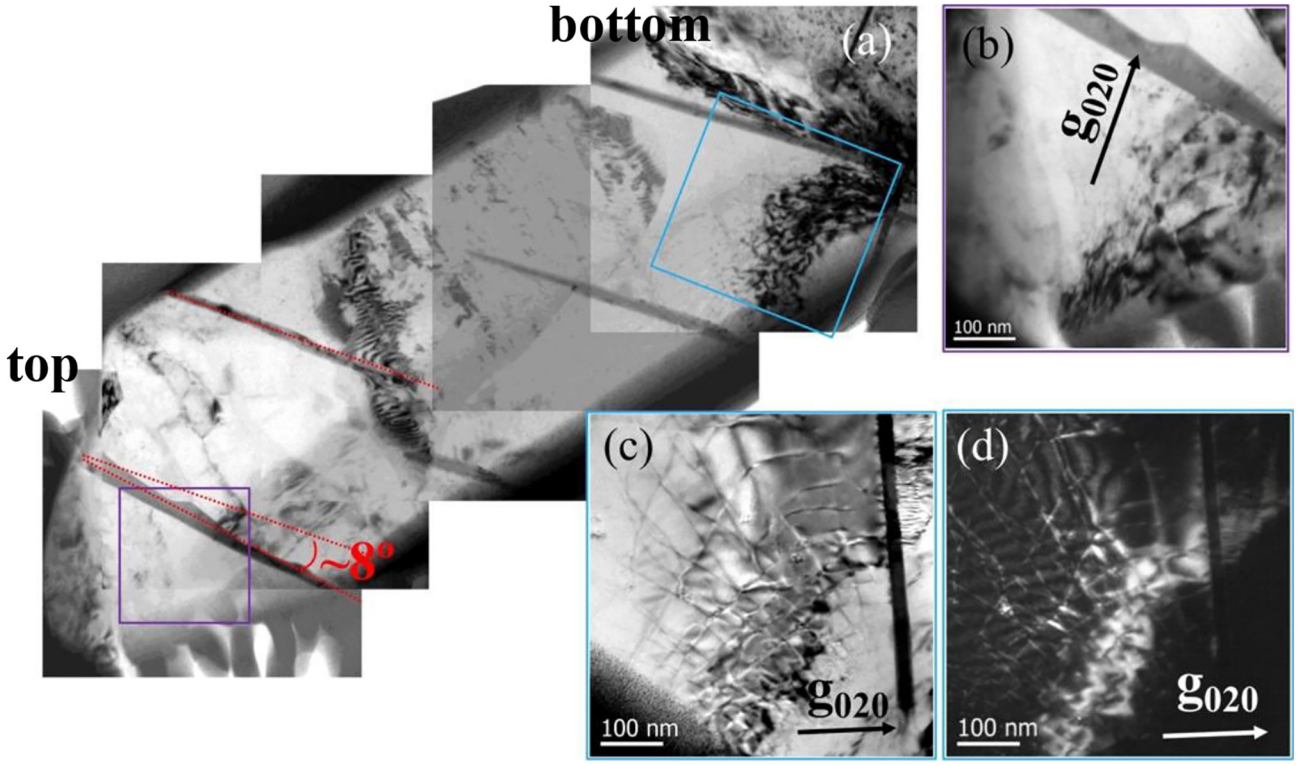

Fig. 9. TEM images of a deformed Al-4.0Cu micro-pillar with {100}-slip traces. (a) The cross section of the micro-pillar observed along [001]-direction. A ~8° rotation for the marked precipitate indicates a strong strain gradient in this region. (b) and (c) are the bright-field TEM images of the regions marked respectively on the left and right part of (a). The irregular shape of θ'-Al_2Cu precipitates can be seen in (b). (d) is the corresponding weak beam dark-field image of (c). The dislocation networks can be observed near the precipitate in (b), (c) and (d).

6. Conclusions

We performed micro-compression tests on [110]-oriented Al-Cu alloys micro-pillars containing plate-like θ'-Al_2Cu precipitates. The microstructural length scales of precipitates are of the order of micrometer, commensurate with the external size L of micro-pillars. Plastic fluctuations, yield strength and deformation mechanisms were investigated. Our results revealed that:

(1) Plastic fluctuations can be effectively inhibited by plate-like precipitates. Translating the pinning strength into an internal length scale

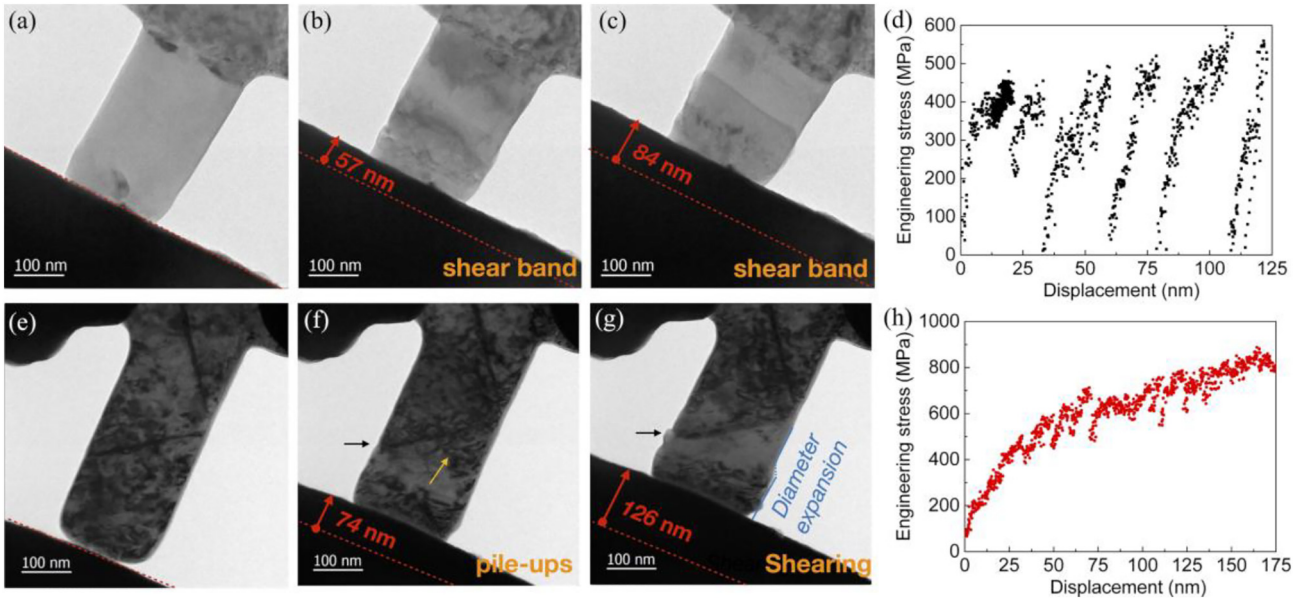

Fig. 10. In-situ observations of deformation behaviors of Al-2.5Cu micro-pillars. (a), (b) and (c) TEM images of a micro-pillar without precipitates. The formation of a large slip band can be identified in (b) and (c). (d) Corresponding engineering stress-displacement curve. (e), (f) and (g) TEM images of a micro-pillar containing two orthorhombic precipitates. Dislocation pile-ups against precipitates, marked by a yellow arrow, can be observed in (f). (g) The pile-up dislocations marked in (f) sheared the precipitate, resulting in a precipitate broadening. The slip traces along the precipitates ({100}-plane) are pointed by black arrows in (f) and (g). (h) Corresponding engineering stress-displacement. The tip displacements are marked in the TEM images. (For interpretation of the references to color in this figure legend, the reader is referred to the web version of this article.)

$l = Gb/\tau_{pin}$, the dimensionless ratio $R = L/l$ unifies the wild-to-mild transition, showing that this inhibition of dislocation avalanches results essentially from the pinning effect of precipitates.

(2) In comparison with Al alloys containing dense nm-sized disorders, plastic deformation is wilder in the present Al-Cu alloys with the same pinning strength. We explained this phenomenon as a breakdown of the mean-field pinning picture, which is a specific feature of these Al-Cu alloys with an external size commensurate with precipitate spacing and size.

(3) A sharp decrease of wildness was observed when the plate-like precipitates cut off the entire micro-pillar. This observation suggests a new way to mitigate the "smaller is wilder" effect in the design of small devices.

(4) The universal relation between wildness W and the power-law exponent κ of the size distribution of strain bursts was proved to be truly universal, regardless of the nature of the disorder (pure metal, solutes, precipitates), the ratio between the characteristic scales of disorder and the sample size, or even the nature of the underlying deformation mechanisms.

CRediT authorship contribution statement

Peng Zhang: Investigation, Methodology, Data curation, Formal analysis, Writing - original draft, Writing - review & editing.**Jian-Jun Bian:**Data curation, Writing - review & editing.**Jin-Yu Zhang:**Writing - review & editing.**Gang Liu:**Conceptualization, Supervision, Writing - review & editing.**Jérôme Weiss:**Supervision, Formal analysis, Writing - original draft, Writing - review & editing.**Jun Sun:**Conceptualization, Supervision, Writing - review & editing.

Declaration of competing interest

None.

Acknowledgments

This work was supported by the National Natural Science Foundation of China (Grant Nos. 51621063, 51722104, 51625103, 51790482, 51761135031 and 51571157), the National Key Research and Development Program of China (2017YFA0700701, 2017YFB0702301), the 111 Project 2.0 of China (BP2018008), and the China Postdoctoral Science Foundation (2019M653595). The financial support by the NSFC-ANR joint project SUMMIT (n° 17-CE08-0047, 51761135031) is sincerely acknowledged. We thank ShengWu Guo and YanHai Li for the TEM characterizations. Peng Zhang thanks the financial support from China Scholarship Council.

References

[1] A. Rinaldi, S. Licoccia, E. Traversa, Nanomechanics for MEMS: a structural design perspective, Nanoscale 3 (3) (2011) 811–824.
[2] A. Witvrouw, H.A.C. Tilmans, I. De Wolf, Materials issues in the processing, the operation and the reliability of MEMS, Microelectron. Eng. 76 (1–4) (2004) 245–257.
[3] M.D. Uchic, P.A. Shade, D.M. Dimiduk, Plasticity of micrometer-scale single crystals in compression, Annu. Rev. Mater. Res. 39 (2009) 361–386.
[4] J.R. Greer, J.T.M. De Hosson, Plasticity in small-sized metallic systems: intrinsic versus extrinsic size effect, Prog. Mater. Sci. 56 (6) (2011) 654–724.
[5] R. Maaß, P.M. Derlet, Micro-plasticity and recent insights from intermittent and small-scale plasticity, Acta Mater. 143 (2018) 338–363.
[6] M.D. Uchic, D.M. Dimiduk, J.N. Florando, W.D. Nix, Sample dimensions influence strength and crystal plasticity, Science 305 (5686) (2004) 986–989.
[7] R. Chen, S. Sandlobes, C. Zehnder, X.Q. Zeng, S. Korte-Kerzel, D. Raabe, Deformation mechanisms, activated slip systems and critical resolved shear stresses in an Mg-LPSO alloy studied by micro-pillar compression, Mater. Des. 154 (2018) 203–216.
[8] J.T. Wang, M. Ramajayam, E. Charrault, N. Stanford, Quantification of precipitate hardening of twin nucleation and growth in Mg and Mg-5Zn using micro-pillar compression, Acta Mater. 163 (2019) 68–77.
[9] D. Kiener, A.M. Minor, Source truncation and exhaustion: insights from quantitative in situ TEM tensile testing, Nano Lett. 11 (9) (2011) 3816–3820.
[10] T.A. Parthasarathy, S.I. Rao, D.M. Dimiduk, M.D. Uchic, D.R. Trinkle, Contribution to size effect of yield strength from the stochastics of dislocation source lengths in finite samples, Scr. Mater. 56 (4) (2007) 313–316.
[11] D. Kiener, A.M. Minor, Source-controlled yield and hardening of Cu(100) studied by in situ transmission electron microscopy, Acta Mater. 59 (4) (2011) 1328–1337.
[12] F. Mompiou, M. Legros, A. Sedlmayr, D.S. Gianola, D. Caillard, O. Kraft, Source-based strengthening of sub-micrometer Al fibers, Acta Mater. 60 (3) (2012) 977–983.
[13] J.R. Greer, W.C. Oliver, W.D. Nix, Size dependence of mechanical properties of gold at the micron scale in the absence of strain gradients, Acta Mater. 53 (6) (2005) 1821–1830.
[14] J.R. Greer, W.D. Nix, Nanoscale gold pillars strengthened through dislocation starvation, Phys. Rev. B 73 (24) (2006).
[15] C.P. Frick, B.G. Clark, S. Orso, A.S. Schneider, E. Arzt, Size effect on strength and strain hardening of small-scale [111] nickel compression pillars, Materials Science and Engineering a-Structural Materials Properties Microstructure and Processing 489 (1–2) (2008) 319–329.
[16] C. Chisholm, H. Bei, M.B. Lowry, J. Oh, S.A.S. Asif, O.L. Warren, Z.W. Shan, E.P. George, A.M. Minor, Dislocation starvation and exhaustion hardening in Mo alloy nanofibers, Acta Mater. 60 (5) (2012) 2258–2264.
[17] P. Zhang, O.U. Salman, J.Y. Zhang, G. Liu, J. Weiss, L. Truskinovsky, J. Sun, Taming intermittent plasticity at small scales, Acta Mater. 128 (2017) 351–364.
[18] D.M. Dimiduk, C. Woodward, R. Lesar, M.D. Uchic, Scale-free intermittent flow in crystal plasticity, Science 312 (5777) (2006) 1188–1190.
[19] F.F. Csikor, C. Motz, D. Weygand, M. Zaiser, S. Zapperi, Dislocation avalanches, strain bursts, and the problem of plastic forming at the micrometer scale, Science 318 (5848) (2007) 251–254.
[20] Y. Cui, G. Po, N. Ghoniem, Controlling strain bursts and avalanches at the nano- to micrometer scale, Phys. Rev. Lett. 117 (15) (2016), 155502.
[21] J.M. Wheeler, L. Thilly, A. Morel, A.A. Taylor, A. Montagne, R. Ghisleni, J. Michler, The plasticity of indium antimonide: insights from variable temperature, strain rate jump micro-compression testing, Acta Mater. 106 (2016) 283–289.
[22] J. Weiss, W. Ben Rhouma, S. Deschanel, L. Truskinovsky, Plastic intermittency during cyclic loading: from dislocation patterning to microcrack initiation, Physical Review Materials 3 (2) (2019).
[23] G. Sparks, Y. Cui, G. Po, Q. Rizzardi, J. Marian, R. Maass, Avalanche statistics and the intermittent-to-smooth transition in microplasticity, Physical Review Materials 3 (8) (2019).
[24] Y. Hu, L. Shu, Q. Yang, W. Guo, P.K. Liaw, K.A. Dahmen, J.M. Zuo, Dislocation avalanche mechanism in slowly compressed high entropy alloy nanopillars, Commun. Phys. 1 (2018).
[25] Y. Cui, G. Po, P. Srivastava, K. Jiang, V. Gupta, N. Ghoniem, The role of slow screw dislocations in controlling fast strain avalanche dynamics in body-centered cubic metals, Int. J. Plast. 124 (2020) 117–132.
[26] J. Weiss, F. Louchet, Seismology of plastic deformation, Scr. Mater. 54 (5) (2006) 747–751.
[27] M. Zaiser, Scale invariance in plastic flow of crystalline solids, Adv. Phys. 55 (1–2) (2006) 185–245.
[28] M.C. Miguel, S. Zapperi, Materials science. Fluctuations in plasticity at the microscale, Science 312 (5777) (2006) 1149–1150.
[29] N. Friedman, A.T. Jennings, G. Tsekenis, J.Y. Kim, M. Tao, J.T. Uhl, J.R. Greer, K.A. Dahmen, Statistics of dislocation slip avalanches in nanosized single crystals show tuned critical behavior predicted by a simple mean field model, Phys. Rev. Lett. 109 (9) (2012), 095507.
[30] S. Brinckmann, J.Y. Kim, J.R. Greer, Fundamental differences in mechanical behavior between two types of crystals at the nanoscale, Phys. Rev. Lett. 100 (15) (2008), 155502.
[31] G. Sparks, R. Maass, Shapes and velocity relaxation of dislocation avalanches in Au and Nb microcrystals, Acta Mater. 152 (2018) 86–95.
[32] Y. Pan, H. Wu, X. Wang, Q. Sun, L. Xiao, X. Ding, J. Sun, E.K.H. Salje, Rotatable precipitates change the scale-free to scale dependent statistics in compressed Ti nanopillars, Sci. Rep. 9 (1) (2019) 3778.
[33] H. Gao, Y. Hu, Y. Xuan, J. Li, Y. Yang, R.V. Martinez, C. Li, J. Luo, M. Qi, G.J. Cheng, Nanolithography. Large-scale nanoshaping of ultrasmooth 3D crystalline metallic structures, Science 346 (6215) (2014) 1352–1356.
[34] B. Girault, A.S. Schneider, C.P. Frick, E. Arzt, Strength effects in micropillars of a dispersion strengthened superalloy, Adv. Eng. Mater. 12 (5) (2010) 385–388.
[35] R. Gu, A.H.W. Ngan, Size effect on the deformation behavior of duralumin micropillars, Scr. Mater. 68 (11) (2013) 861–864.
[36] M. Ovaska, L. Laurson, M.J. Alava, Quenched pinning and collective dislocation dynamics, Sci. Rep. 5 (2015), 10580.
[37] R.Z. Valiev, R.K. Islamgaliev, I.V. Alexandrov, Bulk nanostructured materials from severe plastic deformation, Prog. Mater. Sci. 45 (2) (2000) 103–189.
[38] K. Ng, A. Ngan, Effects of trapping dislocations within small crystals on their deformation behavior, Acta Mater. 57 (16) (2009) 4902–4910.
[39] T. Hu, L. Jian, H. Yang, K.K. Ma, T.D. Topping, J. Yee, M.J. Li, A.K. Mukherjee, J.M. Schoenung, E.J. Lavernia, Stabilized plasticity in ultrahigh strength, submicron Al crystals, Acta Mater. 94 (2015) 46–58.
[40] C. Yang, L. Cao, Y. Gao, P. Cheng, P. Zhang, J. Kuang, J. Zhang, G. Liu, J. Sun, Nanostructural Sc-based hierarchy to improve the creep resistance of Al–Cu alloys, Mater. Des. 186 (2020).
[41] J. Weiss, W.B. Rhouma, T. Richeton, S. Dechanel, F. Louchet, L. Truskinovsky, From mild to wild fluctuations in crystal plasticity, Phys. Rev. Lett. 114 (10) (2015), 105504.
[42] Z.W. Shan, R.K. Mishra, S.A. Syed Asif, O.L. Warren, A.M. Minor, Mechanical annealing and source-limited deformation in submicrometre-diameter Ni crystals, Nat. Mater. 7 (2) (2008) 115–119.

[43] S. Lee, J. Jeong, Y. Kim, S.M. Han, D. Kiener, S.H. Oh, FIB-induced dislocations in Al submicron pillars: annihilation by thermal annealing and effects on deformation behavior, Acta Mater. 110 (2016) 283–294.
[44] P.J. Imrich, C. Kirchlechner, D. Kiener, G. Dehm, In situ TEM microcompression of single and bicrystalline samples: insights and limitations, Jom 67 (8) (2015) 1704–1712.
[45] G. Guillonneau, M. Mieszala, J. Wehrs, J. Schwiedrzik, S. Grop, D. Frey, L. Philippe, J.M. Breguet, J. Michler, J.M. Wheeler, Nanomechanical testing at high strain rates: new instrumentation for nanoindentation and microcompression, Mater. Des. 148 (2018) 39–48.
[46] B.A. Chen, G. Liu, R.H. Wang, J.Y. Zhang, L. Jiang, J.J. Song, J. Sun, Effect of interfacial solute segregation on ductile fracture of Al-Cu-Sc alloys, Acta Mater. 61 (5) (2013) 1676–1690.
[47] K.C. Russell, M.F. Ashby, Slip in aluminum crystals containing strong, plate-like particles, Acta Metall. 18 (8) (1970) 891.
[48] C. Calabrese, C. Laird, Cyclic stress—strain response of two-phase alloys part II. Particles not penetrated by dislocations, Materials Science & Engineering 13 (2) (1974) 159–174.
[49] J.F. Nie, B.C. Muddle, Strengthening of an Al-Cu-Sn alloy by deformation-resistant precipitate plates, Acta Mater. 56 (14) (2008) 3490–3501.
[50] H. Liu, Y.P. Gao, L. Qi, Y.Z. Wang, J.F. Nie, Phase-field simulation of Orowan strengthening by coherent precipitate plates in an aluminum alloy, metallurgical and materials transactions a-physical metallurgy and, Mater. Sci. 46a (7) (2015) 3287–3301.
[51] J.P. Hirth, J. Lothe, Theory of Dislocations, J. Wiley, 1968.
[52] S. Thangaraju, M. Heilmaier, B.S. Murty, S.S. Vadlamani, On the estimation of true Hall-Petch constants and their role on the superposition law exponent in Al alloys, Adv. Eng. Mater. 14 (10) (2012) 892–897.
[53] S. Yan, H. Zhou, Q.H. Qin, Microstructure versus size: nano/microscale deformation of solute-strengthening Al alloys via pillar compression tests, Materials Research Letters 7 (2) (2018) 53–59.
[54] Z.J. Wang, Q.J. Li, Z.W. Shan, J. Li, J. Sun, E. Ma, Sample size effects on the large strain bursts in submicron aluminum pillars, Appl. Phys. Lett. 100 (7) (2012) 986.
[55] F. Mompiou, M. Legros, Plasticity mechanisms in sub-micron Al fiber investigated by in situ TEM, Adv. Eng. Mater. 14 (11) (2012) 955–959.
[56] P. Zhang, J.-J. Bian, C. Yang, J.-Y. Zhang, G. Liu, J. Weiss, J. Sun, Plate-like precipitate effects on plasticity of Al-Cu micro-pillar: {100}-interfacial slip, Materialia 7 (2019).
[57] G. Dehm, B.N. Jaya, R. Raghavan, C. Kirchlechner, Overview on micro- and nanomechanical testing: new insights in interface plasticity and fracture at small length scales, Acta Mater. 142 (2018) 248–282.
[58] X. Feng, J. Zhang, K. Wu, X. Liang, G. Liu, J. Sun, Ultrastrong Al0.1CoCrFeNi high-entropy alloys at small scales: effects of stacking faults vs. nanotwins, Nanoscale 10 (28) (2018) 13329–13334.
[59] Y.H. Lai, C.J. Lee, Y.T. Cheng, H.S. Chou, H.M. Chen, X.H. Du, C.I. Chang, J.C. Huang, S.R. Jian, J.S.C. Jang, T.G. Nieh, Bulk and microscale compressive behavior of a Zr-based metallic glass, Scr. Mater. 58 (10) (2008) 890–893.
[60] J.Y. Zhang, G. Liu, S.Y. Lei, J.J. Niu, J. Sun, Transition from homogeneous-like to shear-band deformation in nanolayered crystalline Cu/amorphous Cu-Zr micropillars: intrinsic vs. extrinsic size effect, Acta Mater. 60 (20) (2012) 7183–7196.
[61] H. Bei, S. Shim, G.M. Pharr, E.P. George, Effects of pre-strain on the compressive stress–strain response of Mo-alloy single-crystal micropillars, Acta Mater. 56 (17) (2008) 4762–4770.
[62] N.L. Okamoto, D. Kashioka, T. Hirato, H. Inui, Specimen-and grain-size dependence of compression deformation behavior in nanocrystalline copper, Int. J. Plast. 56 (2014) 173–183.
[63] D.J. Dunstan, A.J. Bushby, The scaling exponent in the size effect of small scale plastic deformation, Int. J. Plast. 40 (2013) 152–162.
[64] D. Kiener, P. Hosemann, S.A. Maloy, A.M. Minor, In situ nanocompression testing of irradiated copper, Nat. Mater. 10 (8) (2011) 608–613.
[65] R. Maas, P.M. Derlet, J.R. Greer, Small-scale plasticity: insights into dislocation avalanche velocities, Scr. Mater. 69 (8) (2013) 586–589.
[66] A. Clauset, C.R. Shalizi, M.E.J. Newman, Power-law distributions in empirical data, SIAM Rev. 51 (4) (2009) 661–703.
[67] K.A. Dahmen, Y. Ben-Zion, J.T. Uhl, Micromechanical model for deformation in solids with universal predictions for stress-strain curves and slip avalanches, Phys. Rev. Lett. 102 (17) (2009), 175501.
[68] P.D. Ispánovity, L. Laurson, M. Zaiser, I. Groma, S. Zapperi, M.J. Alava, Avalanches in 2D dislocation systems: plastic yielding is not depinning, Phys. Rev. Lett. 112 (23) (2014), 235501.
[69] O.U. Salman, L. Truskinovsky, Minimal integer automaton behind crystal plasticity, Phys. Rev. Lett. 106 (17) (2011), 175503.
[70] C.S. Kaira, C. Kantzos, J.J. Williams, V. De Andrade, F. De Carlo, N. Chawla, Microstructural evolution and deformation behavior of Al-Cu alloys: a Transmission X-ray Microscopy (TXM) and micropillar compression study, Acta Mater. 144 (2018) 419–431.
[71] W. Chen, J. Zhang, S. Cao, Y. Pan, M. Huang, Q. Hu, Q. Sun, L. Xiao, J. Sun, Strong deformation anisotropies of ω-precipitates and strengthening mechanisms in Ti-10V-2Fe-3Al alloy micropillars: precipitates shearing vs precipitates disordering, Acta Mater. 117 (2016) 68–80.
[72] Y. Zou, S. Maiti, W. Steurer, R. Spolenak, Size-dependent plasticity in an Nb25Mo25Ta25W25 refractory high-entropy alloy, Acta Mater. 65 (2014) 85–97.
[73] O. Torrents Abad, J.M. Wheeler, J. Michler, A.S. Schneider, E. Arzt, Temperature-dependent size effects on the strength of Ta and W micropillars, Acta Mater. 103 (2016) 483–494.
[74] D. Kiener, C. Motz, T. Schöberl, M. Jenko, G. Dehm, Determination of mechanical properties of copper at the Micron scale, Adv. Eng. Mater. 8 (11) (2006) 1119–1125.
[75] A.H.W. Ngan, K.S. Ng, Transition from deterministic to stochastic deformation, Philos. Mag. 90 (14) (2010) 1937–1954.
[76] K.S. Ng, A.H.W. Ngan, Stochastic nature of plasticity of aluminum micro-pillars, Acta Mater. 56 (8) (2008) 1712–1720.
[77] G. Sparks, R. Maass, Nontrivial scaling exponents of dislocation avalanches in microplasticity, Physical Review Materials 2 (12) (2018).
[78] G. L'Hôte, S. Cazottes, J. Lachambre, M. Montagnat, P. Courtois, J. Weiss, S. Deschanel, Dislocation dynamics during cyclic loading in copper single crystal, Materialia 8 (2019).
[79] K. Chatterjee, A.J. Beaudoin, D.C. Pagan, P.A. Shade, H.T. Philipp, M.W. Tate, S.M. Gruner, P. Kenesei, J.S. Park, Intermittent plasticity in individual grains: a study using high energy x-ray diffraction, Struct Dyn 6 (1) (2019), 014501.
[80] H. Song, D. Dimiduk, S. Papanikolaou, Universality class of nanocrystal plasticity: localization and self-organization in discrete dislocation dynamics, Phys. Rev. Lett. 122 (17) (2019), 178001.
[81] Y. Cui, G. Po, N. Ghoniem, Influence of loading control on strain bursts and dislocation avalanches at the nanometer and micrometer scale, Phys. Rev. B 95 (6) (2017), 064103.
[82] P. Wang, F. Liu, Y. Cui, Z. Liu, S. Qu, Z. Zhuang, Interpreting strain burst in micropillar compression through instability of loading system, Int. J. Plast. 107 (2018) 150–163.
[83] J.A. El-Awady, Unravelling the physics of size-dependent dislocation-mediated plasticity, Nat. Commun. 6 (2015) 5926.
[84] I. Ryu, W. Cai, W.D. Nix, H.J. Gao, Stochastic behaviors in plastic deformation of face-centered cubic micropillars governed by surface nucleation and truncated source operation, Acta Mater. 95 (2015) 176–183.
[85] Y.N. Cui, P. Lin, Z.L. Liu, Z. Zhuang, Theoretical and numerical investigations of single arm dislocation source controlled plastic flow in FCC micropillars, Int. J. Plast. 55 (2014) 279–292.